Fast interaction of atoms with crystal surfaces: coherent lighting

IOP Conf. Series: Journal of Physics: Conf. Series **875** (2017) 012006 doi:10.1088/1742-6596/875/2/012006

Fast interaction of atoms with crystal surfaces: coherent lighting

M.S. Gravielle

Instituto de Astronomía y Física del Espacio (IAFE, UBA-CONICET), casilla de correo 67, sucursal 28, C1428EGA, Buenos Aires, Argentina

Abstract. Quantum coherence of incident waves results essential for the observation of interference patterns in grazing incidence fast atom diffraction (FAD). In this work we investigate the influence of the impact energy and projectile mass on the transversal length of the surface area that is coherently illuminated by the atomic beam, after passing through a collimating aperture. Such a transversal coherence length controls the general features of the interference structures, being here derived by means of the Van Cittert-Zernike theorem. The coherence length is then used to build the initial coherent wave packet within the Surface Initial Value Representation (SIVR) approximation. The SIVR approach is applied to fast He and Ne atoms impinging grazingly on a LiF(001) surface along a low-indexed crystallographic direction. We found that with the same collimating setup, by varying the impact energy we would be able to control the interference mechanism that prevails in FAD patterns, switching between inter-cell and unit-cell interferences. These findings are relevant to use FAD spectra adequately as a surface analysis tool, as well as to choose the appropriate collimating scheme for the observation of interference effects in a given collision system.

E-mail: msilvia@iafe.uba.ar

1. Introduction

Nowadays grazing-incidence fast atom diffraction (GIFAD or FAD) can be considered as one of the most sensitive methods to investigate the morphological and electronic characteristics of ordered surfaces [1, 2]. The first FAD experiments were carried out on insulator crystals [3, 4]. But shortly afterwords, the technique was applied to very different materials, ranging from semiconductors [5, 6] and metals [7, 8] to adsorbate-covered metal surfaces [9], ultrathin films [10], organic molecules on metal substrates [11], and lately, graphene layers [12]. In all cases, the accuracy of the FAD method relies on the observation of well-defined interference structures, and in this regard, the degree of quantum coherence of the incident beam results an essential ingredient.

In recent articles [13–15] it was shown that the size of the collimating aperture strongly affects FAD distributions, making it possible to observe two different mechanisms - Bragg diffraction or supernumerary rainbows - by varying the width of the collimating slit. Such a behavior is related to the transversal length of the surface area that is coherently lighted by the incident wave packet, whose knowledge becomes crucial for an appropriate comparison between experiments and simulations. The extent of the coherently illuminated region depends not only on the collimating setup, but also on the impact energy and the projectile mass. However, all the theoretical results reported in Refs. [14, 15] were obtained by considering the same incidence

condition, i.e., 1 keV He atoms impinging on a LiF(001) surface with the incidence angle $\theta_i = 0.99$ deg. Therefore, in this paper we extend our previous research [14, 15] in order to explore the influence of the energy and mass of the impinging projectile on the visibility of the interference patterns.

To describe the atom-surface scattering we employ the Surface-Initial Value Representation (SIVR) approximation [16], which is a semi-quantum method that has proved to provide a successful representation of experimental FAD patterns for different collision systems [14, 17, 18]. The main advantages of the SIVR approach, in comparison with full-quantum wave-packet-propagation methods, are the following: i) it offers a clear and intuitive description of the physical mechanisms involved in the interference process, and ii) it requires less computational effort to take into account the complete three-dimensional corrugation of the projectile–surface potential. Additionally, in contrast with other methods [10, 19, 20], the SIVR approximation does not need the use of convolutions to smooth the theoretical angular distributions because the size of the incident wave packet is naturally included in the formalism. In our model, the transversal coherence size of the initial wave packet associated with the incident particle is determined from the collimating conditions by making use of the Van Cittert-Zernike theorem [15, 21]. Under certain further assumptions, the complex degree of coherence of the incident beam can be reduced to a simple analytical form [15], which allows us to interpret our results straightforwardly.

The study is here confined to fast He and Ne atoms grazingly impinging on LiF(001) along the $\langle 110 \rangle$ channel. We have chosen this particular incidence direction because it displays a strong corrugation of the potential across the channel, which gives rise to rich FAD patterns. The article is organized as follows: The theoretical formalism is summarized in Sec. 2. Results for different incidence conditions are presented and discussed in Sec. 3, and in Sec. 4 we outline our conclusions. Atomic units (a.u.) are used unless otherwise stated.

2. Theoretical model

Within the SIVR approximation [16], the scattering amplitude per unit of surface area $\mathcal{S}$ for the elastic transition $\mathbf{K}_i \rightarrow \mathbf{K}_f$, $\mathbf{K}_i$ ($\mathbf{K}_f$) being the initial (final) momentum of the atomic projectile, with $|\mathbf{K}_f| = |\mathbf{K}_i|$, reads

$$A_{if}^{(SIVR)} = \frac{1}{\mathcal{S}} \int_{\mathcal{S}} d\mathbf{R}_o \; f_i(\mathbf{R}_o) \int d\mathbf{K}_o \; g_i(\mathbf{K}_o) \; a_{if}^{(SIVR)}(\mathbf{R}_o, \mathbf{K}_o), \tag{1}$$

where the functions $f_i(\mathbf{R}_o)$ and $g_i(\mathbf{K}_o)$ describe the spatial and momentum profiles of the initial wave packet and $a_{if}^{(SIVR)}(\mathbf{R}_o, \mathbf{K}_o)$ is the partial transition amplitude associated with the classical projectile path $\boldsymbol{R}_t \equiv \boldsymbol{R}_t(\mathbf{R}_o, \mathbf{K}_o)$, with $\mathbf{R}_o$ and $\mathbf{K}_o$ being the starting position and momentum, respectively, at the time $t = 0$. The expression of the SIVR partial transition amplitude, as well as details about its derivation can be found in Ref. [16].

In Eq. (1) the spatial and momentum profiles, $f_i(\mathbf{R}_o)$ and $g_i(\mathbf{K}_o)$ respectively, correspond to the initial coherent wave packet at a fixed distance Z_o from the surface, for which the atomic projectile is hardly affected by the surface interaction. The frame of reference is located on the first atomic layer, with the $\widehat{x}$ versor along the incidence channel and the $\hat{z}$ versor oriented perpendicular to the surface, aiming towards the vacuum region. Hence, the starting position at $t = 0$ can be expressed as $\mathbf{R}_o = \mathbf{R}_{os} + Z_o\widehat{z}$, where $\mathbf{R}_{os} = X_o\widehat{x} + Y_o\widehat{y}$ is the component parallel to the surface plane and the normal distance Z_o was chosen as equal to the lattice constant.

In this work, $f_i(\mathbf{R}_{os})$ is derived from the complex degree of coherence corresponding to an atomic beam produced by an extended incoherent quasi-monochromatic source, after passing through a square collimating aperture of size d, oriented perpendicular to $\mathbf{K}_i$ and placed at a long distance from the source and the surface (see Fig. 1) Under such assumption, the function

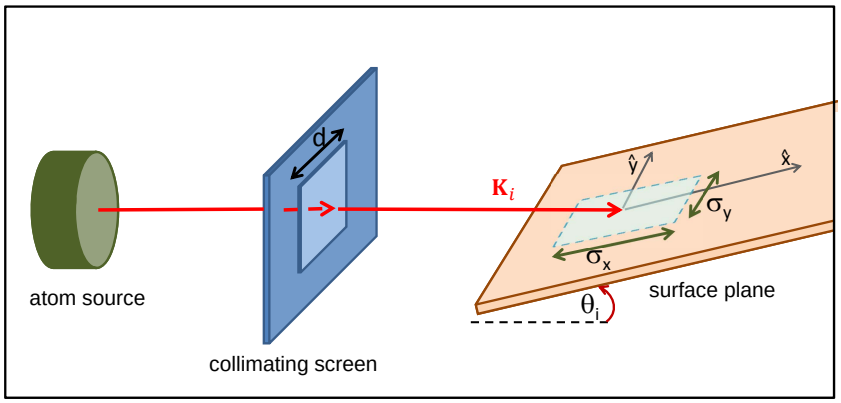

Figure 1. Depiction of the collimating scheme, together with the reference frame.

$f_i(\mathbf{R}_{os})$, obtained by applying the Van Cittert-Zernike theorem [21, 22], can be approximate by means of Gaussian functions $G\left[\omega, x\right] = \left[2/(\pi\omega^2)\right]^{1/4} \exp(-x^2/\omega^2)$ as [14, 15]

$$f_i(\mathbf{R}_{os}) \simeq G\left[\sigma_x, X_o\right] G\left[\sigma_y, Y_o\right], \tag{2}$$

where

$$\sigma_x = \frac{L_c \lambda_\perp}{\sqrt{2}d}, \qquad \sigma_y = \frac{L_c \lambda}{\sqrt{2}d}, \tag{3}$$

denote the *transversal coherence lengths* of the initial coherent wave packet [23] along the $\widehat{x}$- and $\widehat{y}$- directions, respectively. In Eq. (3), L_c is the collimator-surface distance, $\lambda = 2\pi/K_i$ is the de Broglie wavelength of the impinging atom, and $\lambda_\perp = \lambda/\sin\theta_i$ is the perpendicular wavelength associated with the initial motion normal to the surface plane, with θ_i being the polar incidence angle, measured with respect to the surface plane.

The momentum profile $g_i(\mathbf{K}_o)$ is derived from the spatial profile by applying the Heisenberg uncertainty relation [24], reading

$$g_i(\mathbf{K}_o) \simeq g_i(\Omega_o) = G(\omega_\theta, \theta_o - \theta_i) G(\omega_\varphi, \varphi_o), \tag{4}$$

where $\Omega_o \equiv (\theta_o, \varphi_o)$ is the solid angle associated with the $\mathbf{K}_o$- direction, $K_0 = K_i$, and $\omega_\theta = \omega_\varphi = d/(\sqrt{2}L_c)$ [14].

The differential scattering probability in the direction of the solid angle Ω_f is obtained from Eq. (1) as $dP^{(SIVR)}/d\Omega_f = K_f^2 \left| A_{if}^{(SIVR)} \right|^2$, where $\Omega_f \equiv (\theta_f, \varphi_f)$ indicates the direction of $\mathbf{K}_f$, with θ_f the final polar angle, measured with respect to the surface, and φ_f the azimuthal angle, measured with respect to the $\widehat{x}$ axis.

3. Results

In Refs. [14, 15] the influence of the size of a rectangular collimating aperture on FAD distributions was investigated by maintaining fixed incidence conditions. Then, the aim of this work is to widen the scope of the previous research by varying the impact energy and the projectile mass, while the size of the collimating opening remains now unchanged. For this purpose, we consider a collimating configuration similar to the one depicted in Fig. 1, with a square collimating aperture with size $d = 0.2$ mm, placed at a distance $L_c = 25$ cm from the surface plane. These values are in agreement with ordinary collimating setups for FAD [13], while the source parameters were chosen within the validity range of Eq. (2) [15]. That is, the

size of the extended incoherent beam source and its distance to the collimator were estimated as $e \simeq 1$ cm and $L_e \simeq 100$ cm, respectively.

Concerning the collision system, we examine projectile distributions for ^{4}He and ^{20}Ne atoms elastically scattered from LiF(001) along the $< 110 >$ channel. For both projectiles the surface-atom interaction was evaluated with an improved pairwise additive potential [18], which includes non-local terms of the electronic density in the kinetic, exchange and correlation energies. The potential model also takes into account projectile polarization and rumpling effects. Details of the potential model are given in Ref. [18].

In a typical FAD experiment, the fast motion of the projectile along the incidence channel is, on a first approach, sensitive only to the average potential in this direction. Thence, FAD patterns are essentially produced by the slow motion of the projectile in the perpendicular plane, which is governed by the normal energy $E_\perp = E \sin^2\theta_i$, with $E = K_i^2/(2m_P)$ being the total impact energy. In Fig. 2 (a) we show $dP^{(SIVR)}/d\Omega_f$, as a function of θ_f and φ_f, for He projectiles passing through the collimating opening with a normal energy $E_\perp = 0.5$ eV and different total energies, ranging from 0.6 to 8 keV. Due to the energy conservation, each projectile distribution of Fig. 2 (a) lies inside an annulus of radius θ_i, verifying that the higher the energy, the smaller the radius of the angular spectrum [1, 25]. Besides, since neither inelastic processes nor the detector resolution function were taken into account in the present SIVR calculations, for a given $E_\perp$- value all the angular distributions are expected to display the same number of interference peaks, independently of E [26]. However, contrary to such a presumption, from Fig. 2 (a) it is clearly observed that the number and relative intensities of FAD maxima depend strongly on the total impact energy. This behavior is related to the number n_y of reduced unit cells of the crystal surface across the incidence direction that are coherently illuminated by the atomic beam, as it will be explained below.

Under the current collimating conditions, n_y can be roughly estimated from the transversal coherence length of the incident wave packet as

$$n_y = \frac{\sqrt{2}L_c}{d}\frac{\lambda}{a_y}\,, \tag{5}$$

where a_y denotes the width of the incidence channel and σ_y is given by Eq. (3). Hence, the value of n_y varies with the impact energy through its dependence on λ, affecting the general shape of the interference patterns of Fig. 2 (a). For the lowest energy, $E = 0.6$ keV, approximately $n_y \simeq 3.6$ reduced unit cells in the transversal direction are coherently lighted by the He beam, which gives rise to a projectile distribution with well separated Bragg peaks associated with inter-cell interference [27]. But when E augments, and consequently, n_y decreases, these Bragg peaks start to broaden [27], causing that the interference maxima for $E = 2$ keV become comparatively wider than those for $E = 0.6$ keV. In Fig. 2 (a) the limit case for the inter- cell interference corresponds to the total energy $E = 8$ keV, for which a single reduced unit cell results coherently illuminated in the $\widehat{y}$- direction. For this total energy, Bragg peaks vanish completely and only supernumerary rainbow maxima are present in the angular distribution [25].

In order to investigate thoroughly the dependence on E, in Fig. 2 (b) we plot the SIVR probability as a function of the deflection angle $\Theta = \arctan(\varphi_f\ /\theta_f)$ for the cases of Fig. 2 (a). Within the SIVR method the interference mechanisms corresponding to Bragg diffraction and supernumerary rainbows are represented by means of two different factors of the transition amplitude [16]: an inter-cell (Bragg) factor, which is produced by the interference of equivalent trajectories coming from different reduced unit cells across the incidence channel, and a unit-cell factor due to the interference among trajectories coming from one reduced unit cell. The inter-cell factor displays equal-intensity peaks placed at the angular positions Θ_m given by $\sin\Theta_m \cong m\lambda_\perp/a_y$, with $m = 0, \pm1, \pm2, ..,$ which correspond to Bragg angles, indicated

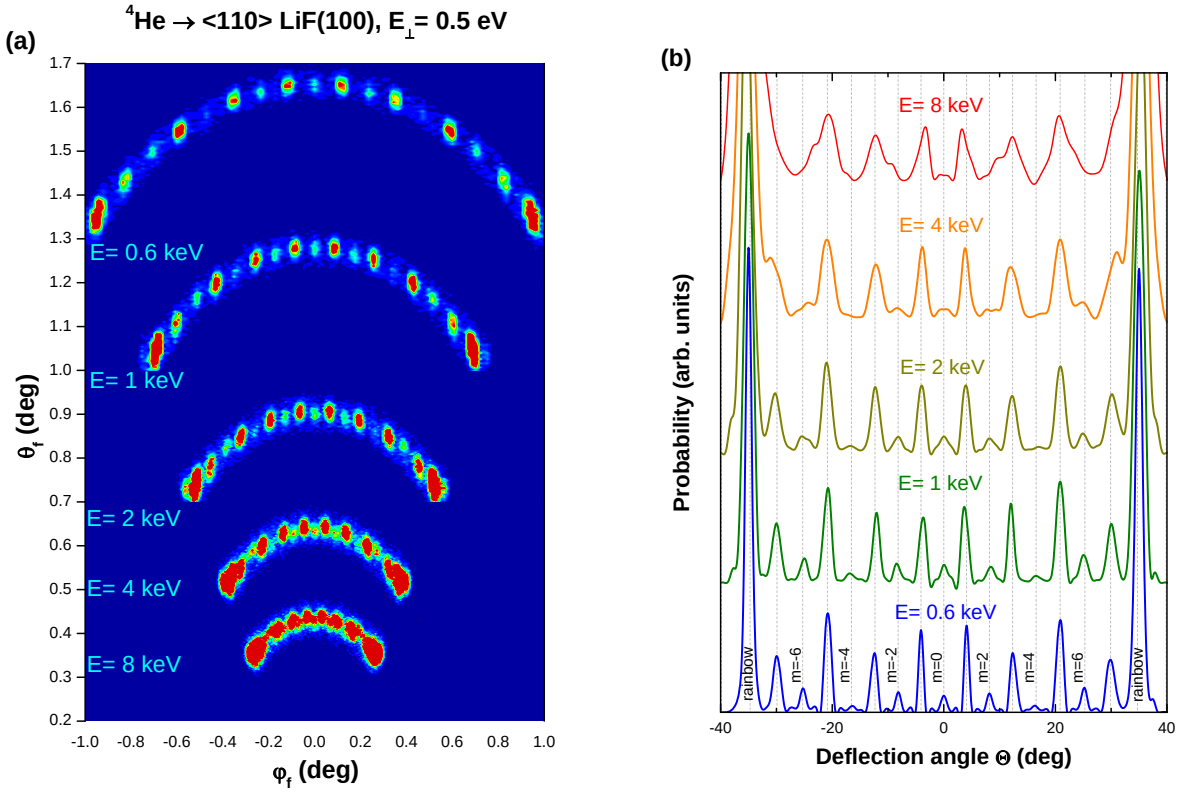

Figure 2. (Color online) Angular spectra for He atoms impinging on LiF(001) along the $\langle 110 \rangle$ direction, with $E_\perp = 0.5$ eV. (a) Two-dimensional distributions, as a function of θ_f and φ_f; and (b) differential probabilities, as a function of the deflection angle Θ. Dashed vertical lines, Θ_m-positions of Bragg angles, as defined in the text.

by vertical dashed lines in Fig. 2 (b). Instead, the unit-cell factor acts as an oscillatory envelope function that modulates the intensity of Bragg peaks, presenting maxima related to supernumerary rainbows [25], like the ones observed in the projectile distribution for $E = 8$ keV at the top of Fig. 2 (b). In addition, all the spectra of Fig. 2 (b) display sharp rainbow maxima at the outermost angles, which have a classical origin.

In elastic He-LiF FAD processes, Θ- positions and relative intensities of the interference peaks were proved to be independent of E at the same $E_\perp$ [26, 27]. Nevertheless, in Fig. 2 (b) we remarkably found that the projectile distributions, as a function of the deflection angle, are strongly affected by the total energy if the same collimating setup is used in all the cases. Then, these results indicate that by increasing E while keeping invariable the normal energy and the collimation conditions, it would be possible to modify gradually the interference patterns, switching from Bragg peaks, with intensities sculpted by the unit-cell factor, as it happens for $E = 0.6$ keV in Fig. 2 (b), to *pure* supernumerary rainbow maxima, where the inter-cell interference is completely erased, as observed for $E = 8$ keV. We stress that this effect is mainly produced by the variation of the parameter n_y associated with the transversal coherence length, rather than by thermally displaced lattice atoms or the spatial resolution of the detector, as it was previously suggested [1].

An analogous behavior is displayed by the two-dimensional projectile distributions of Fig. 3 corresponding to Ne atoms scattered off LiF(001), after crossing the collimating aperture. For Ne projectiles the n_y-dependence on the atomic mass, through the de Broglie wavelength

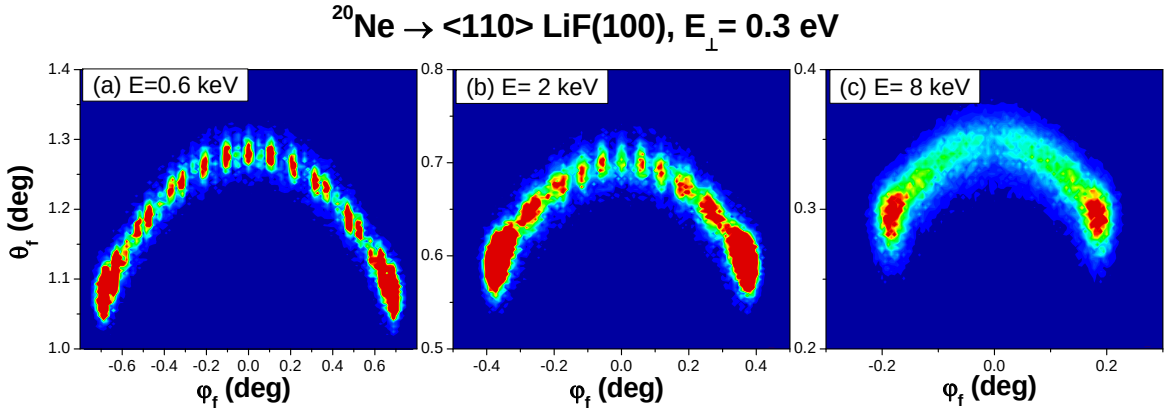

Figure 3. (Color online) Two-dimensional projectile distributions, as a function of θ_f and φ_f, for Ne atoms impinging on LiF(001) along the $\langle 110 \rangle$ direction, with $E_\perp = 0.3$ eV.

[Eq. (5)], originates a reduction of the number of coherently lighted cells in comparison with He at the same impact energy. Therefore, in Fig. 3 (a) the angular distribution for 0.6 keV Ne atoms shows not fully resolved Bragg peaks, in contrast with the corresponding spectrum for He [Fig. 2 (a)]. Furthermore, under present collimation conditions the limit energy for the observation of inter-cell interferences in Ne spectra results to be about 5 times lower than in the case of He impact. Hence, the Ne spectrum for $E = 2$ keV [Fig. 3 (b)] displays only supernumerary rainbow maxima, in accord with the estimated value $n_y \simeq 0.9$. In turn, in this case all the interference signatures start to blur out for $E \gtrapprox 4$ keV, and for $E = 8$ keV only a small portion of the unit-cell (i.e., $n_y \simeq 0.4$) results coherently lighted by the incident beam. This fact washes up the quantum interference, making the angular distribution of Fig. 3 (c) tend to the classic limit, where only rainbow maxima are present. Again these results suggest that the transversal coherence length is the main parameter that determines the observation of Bragg or supernumerary rainbow peaks in FAD spectra, while other contributions, like thermal vibrations of lattice atoms or the detector resolution [28], might play a secondary role.

4. Conclusions

We have investigated the influence of the total energy and the projectile mass on the complex degree of coherence of an atomic beam that impinges grazingly on the crystal surface, after passing through a fixed collimating setup. In our model, the complex degree of coherence determines the transversal coherence length of the initial wave packet, which governs the general features of FAD patterns. We found that, even using the same collimating aperture, it is possible to produce final projectile distributions containing different interference structures - Bragg peaks or supernumerary rainbow maxima - by varying the total energy while keeping the normal energy as a constant. This behavior can be explained in terms of the number n_y of reduced unit cells of the crystal surface across the incidence direction that are coherently illuminated by the atomic beam. The decreasing of n_y as E increases originates the gradually broadening of Bragg peaks, until they fade completely for $n_y \simeq 1$, bringing to light the unit-cell interference associated with supernumerary rainbow maxima.

The energy ranges corresponding to these interference mechanisms depend on the projectile mass through the de Broglie wavelength. For Ne projectiles, the value $n_y \simeq 1$ corresponding to a *pure* unit-cell interference is reached at a total energy lower than for He projectiles, and for higher energies all the interference structures become blurred out, tending to the classical

distribution where only rainbow peaks are present.

Lastly, even though these findings are waiting for experimental confirmation, they can be useful to guide future experiments on coherent lighting for a wide variety of collision processes, involving not only surfaces but also clusters and molecules as targets.

Acknowledgments

This work was carried out with financial support of CONICET and ANPCyT of Argentina.

References

[1] Winter H and Schüller A 2011 *Prog. Surf. Sci.* **86** 169–221
[2] Debiossac M, Atkinson P, Zugarramurdi A, Eddrief M, Finocchi F, Etgens V H, Momeni A, Khemliche H, Borisov A G and Roncin P 2017 *Appl. Surf. Sci.* **391** 53–58
[3] Schüller A, Wethekam S and Winter H 2007 *Phys. Rev. Lett.* **98** 016103
[4] Rousseau P, Khemliche H, Borisov A G and Roncin P 2007 *Phys. Rev. Lett.* **98** 016104
[5] Khemliche H, Rousseau P, Roncin P, Etgens V H and Finocchi F 2009 *Appl. Phys. Lett.* **95** 151901
[6] Debiossac M, Zugarramurdi A, Khemliche H, Roncin P, Borisov A G, Momeni A, Atkinson P, Eddrief M, Finocchi F and Etgens V H 2014 *Phys. Rev. B* **90** 155308
[7] Bundaleski N, Khemliche H, Soulisse P and Roncin P 2008 *Phys. Rev. Lett.* **101** 177601
[8] Busch M, Schüller A, Wethekam S and Winter H 2009 *Surf. Sci.* **603** L23–L26
[9] Schüller A, Busch M, Wethekam S and Winter H 2009 *Phys. Rev. Lett.* **102** 017602
[10] Seifert J, Schüller A, Winter H, Włodarczyk R, Sauer J and Sierka M 2010 *Phys. Rev. B* **82** 035436
[11] Seifert J, Busch M, Meyer E and Winter H 2013 *Phys. Rev. Lett.* **111** 137601
[12] Zugarramurdi A, Debiossac M, Lunca-Popa P, Mayne A J, Momeni A, Borisov A G, Mu Z, Roncin P and Khemliche H 2015 *Appl. Phys. Lett.* **106** 101902
[13] Seifert J, Lienemann J, Schüller A and Winter H 2015 *Nucl. Instrum. Methods Phys. Res. B* **350** 99–105
[14] Gravielle M S and Miraglia J E 2015 *Phys. Rev. A* **92** 062709
[15] Gravielle M S and Miraglia J E 2016 *Nucl. Instrum. Methods Phys. Res. B* **382** 42–48
[16] Gravielle M S and Miraglia J E 2014 *Phys. Rev. A* **90** 052718
[17] Bocan G A, Fuhr J D and Gravielle M S 2016 *Phys. Rev. A* **94** 022711
[18] Miraglia J E and Gravielle M S 2017 *Phys. Rev. A* **95** 022710
[19] Zugarramurdi A and Borisov A G 2013 *Nucl. Instr. Methods Phys. Res. B* **317** 83–89
[20] Rubiano C A R, Bocan G A, Gravielle M S, Bundaleski N, Khemliche H and Roncin P 2013 *Phys. Rev. A* **87** 012903
[21] Born M and Wolf E 1986 *Principles of Optics* (Oxford: Pergamon Press) p Chap. 10
[22] Schaff J F, Langen T and Schmiedmayer J 2014 *Riv. Nuovo Cimento* **37** 509–589
[23] Tonomura A 1986 *Electron Holography* vol 23 (Amsterdam: North-Holland) pp 183–220
[24] Cohen-Tannoudji C, Diu B and Laloë F 2011 *Quantum Mechanics* (Paris: Willey-VCH) p Chapter I
[25] Schüller A and Winter H 2008 *Phys. Rev. Lett.* **100** 097602
[26] Schüller A, Winter H, Gravielle M S, Pruneda J M and Miraglia J E 2009 *Phys. Rev. A* **80** 062903
[27] Gravielle M S 2015 *J. Phys. Conf. Ser.* **583** 012027
[28] Gravielle M S, Schüller A, Winter H and Miraglia J E 2011 *Nucl. Instr. Methods Phys. Res. B* **269** 1208–1211